Journal of Power Sources 188 (2009) 433–446

Contents lists available at ScienceDirect

Journal of Power Sources

journal homepage: www.elsevier.com/locate/jpowsour

Numerical investigations of effect of membrane electrode assembly structure on water crossover in a liquid-feed direct methanol fuel cell

W.W. Yang, T.S. Zhao*

Department of Mechanical Engineering, The Hong Kong University of Science and Technology, Clear Water Bay, Kowloon, Hong Kong SAR, China

ARTICLE INFO

Article history:
Received 6 October 2008
Received in revised form 5 November 2008
Accepted 19 November 2008
Available online 13 December 2008

Keywords:
Direct methanol fuel cell
Membrane electrode assembly
Water crossover
Two-phase
Mass-transport model
Back-flow flux
Convection flux

ABSTRACT

A two-phase mass-transport model is employed to investigate the water transport behaviour through the membrane electrode assembly (MEA) of a liquid-feed direct methanol fuel cell (DMFC). Emphasis is placed on examining the effects of each constituent component design of the MEA, including catalyst layers, microporous layers and membranes, on each of the three water crossover mechanisms: electro-osmotic drag, diffusion, and convection. The results show that lowering the diffusion flux of water or enhancing the convection flux of water (termed as the back-flow flux) through the membrane are both feasible to suppress water crossover in DMFCs. It is found that the reduction in the diffusion flux of water can be mainly achieved through optimum design of the anode porous layers, as the effect of the cathode porous region on water crossover by diffusion is relatively smaller. On the other hand, the design of the cathode porous layers plays a more important role in increasing the back-flow flux of water from the cathode to anode.

1. Introduction

Proper water management is of vital importance to ensure stable, reliable and high performance of direct methanol fuel cells (DMFCs) [1–3]. Although there are great similarities in DMFCs and gas-hydrogen-fed polymer electrolyte fuel cells (PEFCs), water management in DMFCs appears to be different from that in PEFCs. In DMFCs, as a liquid methanol solution is fed to the anode, sufficient membrane hydration can be maintained. Hence, unlike in PEFCs, no external humidifying device is needed in liquid-feed DMFCs. However, a penalty associated with the liquid fuel feed at the anode is the high rate of water crossover to the cathode, that causes two problems for DMFC technology [4–13]. First, it results in a water loss from the anode and thus make-up water is needed, especially for passive DMFCs [10–13]. Second, a high rate of water crossover to the cathode may exaggerate the cathode water flooding problem, and there by limit the cathode performance. Therefore, suppressing water crossover is important not only to simplify the DMFC system but also to improve cell performance. To reduce the rate of water crossover, it is essential to gain a better understanding of water transport through the MEA structure.

The problem of water crossover through DMFC membranes has been studied extensively over the past decade [4–21]. Ren et al. [4–5] were among the pioneers who measured the electro-osmotic drag coefficient of water in DMFC membranes. It was found that the water transport property in DMFC membranes was much higher than that in PEFC membranes. Modelling of water transport through a single membrane and the entire membrane electrode assembly of the DMFC was also performed [6–9]. Subsequently, some innovative designs of the MEA structure were proposed [10–15] to achieve low water crossover and even a water-neutral operation condition [10–11] in DMFCs. In the previous designs, the main idea of reducing water crossover was to increase the hydrophobic level and reduce the pore size of the cathode microporous layer (MPL), which helps build up a high cathode liquid pressure to enhance the water back-flow to the anode. For instance, Peled et al. [10–11] found the use of a highly hydrophobic cathode MPL made it possible to operate a passive DMFC under water-neutral operating conditions. Jewett et al. [13] tested the effect of the cathode gas-diffusion layer (GDL) on water crossover from the anode to the cathode in a miniature passive DMFC, and found that the rate of water crossover could be reduced by adding two additional hydrophobic gas-diffusion layers to the cathode. Lu et al. [14] reported a novel MEA design consisting of a thin membrane and a GDL coated with a MPL. The buildup of liquid pressure in the cathode that resulted from the large contact angle and the small pore size of the MPL created the back-flow flux of water from the cathode to the anode, which substantially reduced the rate of water crossover. Recently, a similar MEA design was also reported by Liu et al. [15] to suppress both methanol and water crossover through the membrane. Additionally, water crossover in single DMFCs and DMFC stacks were experimentally quantified by researchers [16–18]. An approach that enabled in-situ

* Corresponding author. Tel.: +852 2358 8647 fax: +852 2358 1543.
E-mail address: metzhao@ust.hk (T.S. Zhao).

0378-7753/$ – see front matter © 2008 Elsevier B.V. All rights reserved.
doi:10.1016/j.jpowsour.2008.11.139

Nomenclature

A_{lg}	interfacial specific area between liquid and gas phase ($m^2\ m^{-3}$)
A_s	specific surface area of the active reaction sites ($m^2\ m^{-3}$)
C	molar concentration ($mol\ m^{-3}$)
D	diffusivity ($m^2\ s^{-1}$)
F	faraday constant (96,478 $C\ mol^{-1}$)
h_{lg}	interfacial transfer rate constant for methanol ($m\ s^{-1}$)
I_{cell}	cell current density ($A\ m^{-2}$)
I_{para}	parasitic current resulting from methanol crossover ($A\ m^{-2}$)
j_0	exchange current density ($A\ m^{-2}$)
j_a	anode current density ($A\ m^{-3}$)
j_c	cathode current density ($A\ m^{-3}$)
k_c	condensation rate ($mol\ atm^{-1}\ s^{-1}\ m^{-3}$)
k_e	evaporation rate ($1\ atm^{-1}\ s^{-1}$)
k_H	Henry's law constant (Pa)
k_r	relative permeability
K	permeability of porous material (m^2)
$\dot{m}$	source term in mass conservation equation ($kg\ m^{-3}\ s^{-1}$)
M	molecular weight ($kg\ mol^{-1}$)
N	mol flux ($mol\ m^{-2}\ s^{-1}$)
n_d	electro-osmotic drag coefficient
p_c	capillary pressure (Pa)
p_g	gas phase pressure (Pa)
p_l	liquid phase pressure (Pa)
R	gas constant ($J\ mol^{-1}\ K^{-1}$)
$\dot{R}$	source term in species conservation equation ($mol\ m^{-3}\ s^{-1}$)
$\tilde{R}$	interfacial species transfer rate ($mol\ m^{-3}\ s^{-1}$)
$R_{contact}$	Ohmic contact resistance ($\Omega\ m^2$)
s	liquid saturation
T	temperature (K)
V_0	thermodynamic equilibrium voltage, V
V_{cell}	cell voltage (V)
x	coordinate, m, or mole fraction in liquid solution
y	mole fraction in gas phase

Greek

α_a	anode transfer coefficient at anode
α_c	cathode transfer coefficient at cathode
γ	reaction order
δ	thickness of porous layer, m
ε	porosity of porous medium
λ	water content
η	overpotential (V)
κ	ionic conductivity of membrane ($\Omega^{-1}\ m^{-1}$)
μ	viscosity ($kg\ m^{-1}\ s^{-1}$)
θ_c	contact angle (°)
ρ	density ($kg\ m^{-3}$)
σ	interfacial tension ($N\ m^{-1}$)

Superscripts

eff	effective value
in	inlet condition
ref	reference value
sat	saturated value

Subscripts

a	anode
c	cathode
cl	catalyst layer
con	convection
diff	diffusion
dl	diffusion layer
dry	dry membrane
eo	electro-osmotic
eq	equilibrium
g	gas phase
l	liquid phase
mem	membrane
mpl	micro-porous layer
M	methanol
MV	methanol vapour
N	nafion
W	water
WV	water vapour

measurement of the water-crossover rate in a DMFC was proposed by Xu and Zhao [18]. With this method, the mechanisms that lead to water crossover and the effects of various design variables of the MEA and cell operating conditions were investigated. The study showed that the rate of water crossover was dominated by the water diffusion transport due to a large water-concentration gradient across the membrane, especially at relatively low current densities. In addition, the study also highlighted the important role of the hydrophobic cathode MPL in reducing water crossover. More recently, the effects of the cathode backing layer and cathode MPL on the transport behaviour of both water and oxygen were investigated [19–20]. The results suggested that an optimum design of the cathode gas-diffusion layer was crucial to reduce water crossover and simultaneously ensure sufficient supply of oxygen. It should be mentioned that most of the previous work focused on the effect of the cathode GDL on water crossover [10–15,18–20], whereas there are very few studies of the role of the anode GDL in the water management of the DMFC. Very recently, Liu et al. [21] examined the effect of various design variables of the anode MPL on water crossover in a DMFC. They showed that the wettability of the anode MPL had a significant impact on water crossover. The MEA with a hydrophobic anode MPL led to a reduction in the rate of water crossover compared with a hydrophilic one.

A literature review suggests that extensive efforts have been devoted to explore the influence of the cathode GDL (the backing layer and MPL) on water crossover in DMFCs [10–15,18–20]. However, at present the role of the anode porous structure in water management is still far from understood. In this work, we have numerically studied water transport behaviour through the MEA of a liquid-fed DMFC. Emphasis is placed on examining the effects of all the constituent components of the MEA, including the anode catalyst layer, the anode MPL, the membrane, the cathode catalyst layer and the cathode MPL, on water crossover.

2. Mathematical model

We consider a MEA, as illustrated in Fig. 1, which consists of seven layers from the interface I between the anode channel and anode diffusion layer to the interface VIII between the cathode diffusion layer and cathode channel. Notice that micro-porous layers (MPLs) are also included between the catalyst layers (CLs) and the coarse diffusion layers (DLs) at both the anode and the cathode. Due to the coexistence of liquid and gas phases in the constituent components of the DMFC under typical operating conditions, a two-phase mass-transport model, as outlined below, is used to study the water transport behaviour through the MEA of the DMFC. More

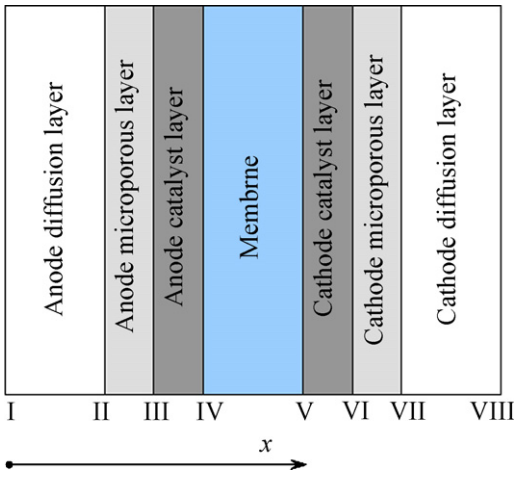

Fig. 1. Schematic of model domain.

details about the development of the two-phase mass-transport model can be found elsewhere [20,22–24].

2.1. Governing equations for mass-transport

We now present the governing equations for the steady-state, isothermal two-phase mass-transport in the porous anode and cathode of the DMFC, as well as for the dissolved water and methanol transport through the membrane. Referring to Fig. 1, in the anode (from interface I–IV) and cathode porous regions (from V to VIII), there are a total of eight variables involved, namely liquid pressure in the anode ($p_{l,a}$), gas pressure in the anode ($p_{g,a}$), the concentration of liquid methanol ($C_{M,L}$), the concentration of methanol vapour ($C_{M,g}$), liquid phase pressure in the cathode ($p_{l,c}$), gas phase pressure in the cathode ($p_{g,c}$), the concentration of gas oxygen in the cathode ($C_{O_2,g}$), and the concentration of water vapour in the cathode ($C_{WV,g,c}$). In the membrane (from interface IV to interface V), the variables that are considered are the dissolved methanol concentration ($C_{M,N}$) and the dissolved water concentration ($C_{W,N}$). The corresponding governing equations are presented below:

Anode porous region (I–IV)

$$p_{l,a}: \quad \nabla\left(-\frac{Kk_{rl}}{\mu_l/\rho_l}\nabla p_{l,a}\right) = \dot{m}_{l,a} \tag{1}$$

$$p_{g,a}: \quad \nabla\left(-\frac{Kk_{rg}}{\mu_g/\rho_g}\nabla p_{g,a}\right) = \dot{m}_{g,a} \tag{2}$$

$$C_{M,l}: \quad \nabla\left[\left(-\frac{Kk_{rl}}{\mu_l}\nabla p_l\right)C_{M,l} - D^{eff}_{M,l}\nabla C_{M,l}\right] = \dot{R}_{M,l} \tag{3}$$

$$C_{MV,g}: \quad \nabla\left[\left(-\frac{Kk_{rg}}{\mu_g}\nabla p_g\right)C_{MV,g} - D^{eff}_{MV,g}\nabla C_{MV,g}\right] = \dot{R}_{MV,g} \tag{4}$$

Cathode porous region (V–VIII)

$$p_{l,c}: \quad \nabla\left[\left(-\frac{Kk_{rl}}{\mu_l/\rho_l}\right)\nabla p_{l,c}\right] = \dot{m}_{l,c} \tag{5}$$

$$p_{g,c}: \quad \nabla\left[\left(-\frac{Kk_{rg}}{\mu_g/\rho_g}\right)\nabla p_{g,c}\right] = \dot{m}_{g,c} \tag{6}$$

$$C_{O_2,g}: \quad \nabla\left[\left(-\frac{Kk_{rg}}{\mu_g}\nabla p_{g,c}\right)C_{O_2,g} - D^{eff}_{O_2,g}\nabla C_{O_2,g}\right] = \dot{R}_{O_2,g} \tag{7}$$

$$C_{WV,g,c}: \quad \nabla\left[\left(-\frac{Kk_{rg}}{\mu_g}\nabla p_{g,c}\right)C_{WV,g,c} - D^{eff}_{WV,g}\nabla C_{WV,g,c}\right] = \dot{R}_{WV,g} \tag{8}$$

Noted that the pressure difference between liquid and gas is balanced by a capillary pressure as given by [25]:

$$p_c = p_g - p_l = \sigma\cos\theta_c\left(\frac{\varepsilon}{K}\right)^{0.5}J(s) \tag{9}$$

where σ, θ_c, ε and K denote the surface tension between liquid and gas, the contact angle of the porous medium, the porosity of the porous medium and the intrinsic permeability of the porous medium, respectively. The term $J(s)$ herein is the widely-used Leverett function and written as:

$$J(s) = \begin{cases} 1.417(1-s) - 2.120(1-s)^2 + 1.263(1-s)^3 & 0 < \theta_c \le 90^\circ \\ 1.417s - 2.120s^2 + 1.263s^3 & 90^\circ < \theta_c < 180^\circ \end{cases} \tag{10}$$

with s representing the liquid saturation, i.e., the volume fraction of liquid water that fills pores in the porous medium.

Electrolyte regions (III–VI)

In the polymer electrolyte membrane, transport of dissolved phases (i.e., dissolved methanol and water) needs to be considered. Generally, dissolved methanol transport in the membrane depends on diffusion, convection and electro-osmotic drag. The flux of the dissolved methanol transport through the membrane can be expressed as:

$$N_M = -D^{eff}_M\nabla C_{M,N} + n_{d,}\frac{I}{F} - \left(\frac{K}{\mu_l}\nabla p_l\right)C_{M,N} \tag{11}$$

and the conservation of the dissolved methanol in the membrane is:

$$\nabla N_M = 0 \tag{12}$$

The dissolved water transport through the membrane also depends on diffusion, electro-osmotic drag and convection. Hence, the flux of the dissolved water transport through the membrane can be expressed as:

$$N_W = -D_{W,N}\nabla C_{W,N} + n_{d,H_2O}\frac{I}{F} - \frac{\rho_l}{M_{H_2O}}\frac{K}{\mu_l}\nabla p_l \tag{13}$$

and the conservation of dissolved water in the membrane is:

$$\nabla N_W = 0 \tag{14}$$

The concentration of the dissolved water ($C_{W,N}$) is related to the water content (λ) in the membrane by:

$$C_{W,N} = \frac{\rho_{dry}\lambda}{EW} \tag{15}$$

where ρ_{dry} and EW represent the density of the dry membrane and the equivalent weight of the ionomer in the membrane, respectively.

As for the dissolved water in the polymer electrolyte of the CLs, for simplicity, it is assumed to be in phase equilibrium with the liquid water and water-vapour-saturated gas in the voids of the CLs. As such, the water content in the polymer electrolyte of the CLs can be expressed as:

$$\lambda_{CL} = (1-s)\lambda^{eq}_{WV} + s\lambda^{eq}_{l} \tag{16}$$

where λ^{eq}_{WV} and λ^{eq}_{l} are the equilibrium water contents when the polymer electrolyte is in phase equilibrium with the water-vapour-saturated gas [20] and liquid water, respectively.

2.2. Boundary and interfacial conditions

As indicated in Fig. 1, the model domain is enclosed by eight boundaries/interfaces. The external boundaries (namely, interfaces I and VIII) represent the inlets of the reactant supply at which the variables are all specified to be the inlet conditions, while the internal interfacial conditions in the 'sandwiched' DMFC are given based on the principle that continuity and mass flux balance are required for each interface to satisfy the general mass conservation in the

Table 1
Constitutive correlations.

Parameters	Expressions	
Relative permeabilities	$k_{rl} = s^3$ $k_{rg} = (1-s)^3$	Liquid Gas
Effective diffusion coefficients of species [22]	$D_{i,g}^{eff} = D_{i,g}\varepsilon^{1.5}(1-s)^{1.5}$ i: O_2, WV,MV	
	$D_M^{eff} = \begin{cases} D_{M,l}\varepsilon^{1.5}s^{1.5} \\ \dfrac{(\varepsilon+\varepsilon_N)}{[\varepsilon/(D_{M,l}\varepsilon^{1.5}s^{1.5})+\varepsilon_N/(D_{M,N}\varepsilon_N{}^{1.5})]} \\ D_{M,N}\varepsilon^{1.5} \end{cases}$	ADL/AMPL ACL MEM
General generation rate of mass in liquid phase	$\dot{m}_{l,a} = \begin{cases} -M_M\tilde{R}_M \\ -(M_{H_2O}+M_M)\dfrac{j_a}{6F} - M_M\tilde{R}_M \end{cases}$	ADL/AMPL ACL
	$\dot{m}_{l,c} = \begin{cases} -M_{H_2O}\tilde{R}_w \\ M_{H_2O}\left(\dfrac{j_c}{2F} - \dfrac{I_p}{6F\delta_{ccl}}\right) - M_{H_2O}\tilde{R}_w \end{cases}$	CDL/CMPL CCL
General generation rate of mass in gas phase	$\dot{m}_{g,a} = \begin{cases} M_M\tilde{R}_M \\ M_{CO_2}\dfrac{j_a}{6F} + M_M\tilde{R}_M \end{cases}$	ADL/AMPL ACL
	$\dot{m}_{g,c} = \begin{cases} M_{H_2O}\tilde{R}_w \\ -M_{O_2}\dfrac{j_c}{4F} + M_{CO_2}\dfrac{I_p}{6F\delta_{ccl}} + M_{H_2O}\tilde{R}_w \end{cases}$	CDL/CMPL CCL
Mole generation	$\dot{R}_{O_2} = \begin{cases} 0 \\ -\dfrac{j_c}{4F} \end{cases}, \dot{R}_{WV,c} = \begin{cases} \tilde{R}_w \\ \tilde{R}_w \end{cases}$	CDL/CMPL CCL
Rate of species	$\dot{R}_{M,l} = \begin{cases} -\tilde{R}_M \\ -\dfrac{j_a}{6F} - \tilde{R}_M \end{cases}, \dot{R}_{MV,a} = \begin{cases} \tilde{R}_M \\ \tilde{R}_M \end{cases}$	ADL/AMPL ACL
Interfacial transfer rate of methanol between the liquid and gas phase [33]	$\tilde{R}_M = A_{lg}h_{lg}s(1-s)\frac{(p_{MV}^{sat}-p_{MV})}{RT}$	
Interfacial transfer rate of water between the liquid and gas phase [33]	$\tilde{R}_w = \begin{cases} k_e\dfrac{\varepsilon s\rho_l}{M_{H_2O}}(y_{WV}p_g - p_{WV}^{sat}) & y_{WV}p_g < p_{WV}^{sat} \\ k_c\dfrac{\varepsilon(1-s)y_{WV}}{RT}(y_{WV}p_g - p_{WV}^{sat}) & y_{WV}p_g > p_{WV}^{sat} \end{cases}$	

entire cell. More details of the boundary and interfacial conditions can be found elsewhere [20,22].

2.3. Electrochemical kinetics

At the DMFC anode, the Tafel-like expression is simply used to express the kinetics of the methanol oxidation reaction (MOR):

$$j_a = A_{s,a}j_{0,M}^{ref}\left(\frac{C_M}{C_M^{ref}}\right)^{\gamma}\exp\left(\frac{\alpha_a F}{RT}\eta_a\right) \tag{17}$$

where the reaction order (γ) is related to the methanol concentration and assumed to be zero when the methanol concentration is higher than a reference value [25]. Otherwise, the first-order reaction is specified.

With respect to the oxygen reduction reaction (ORR) on the cathode, the modified first-order Tafel-like kinetics is used, which gives:

$$j_c = (1-s)A_{s,c}j_{0,O_2}^{ref}\left(\frac{C_{O_2}}{C_{O_2}^{ref}}\right)\exp\left(\frac{\alpha_c F}{RT}\eta_c\right) \tag{18}$$

where the term (1 − s) represents a correction factor in view of the adverse impact of the liquid water in the cathode CL on the rate of the ORR [25].

2.4. Water balance

As mentioned above, transport of dissolved water through the membrane depends on diffusion, electro-osmotic drag and convection. The fluxes of water crossover through the membrane by diffusion ($N_{W,diff}$) and electro-osmotic drag ($N_{W,eo}$) are, respectively, determined from:

$$N_{W,diff} = -D_{W,N}(\lambda)\nabla C_{W,N}|_{IV} \tag{19}$$

$$N_{W,eo} = n_{d,H_2O}(\lambda)\frac{I}{F}|_{IV} \tag{20}$$

and the flux of water by back-flow resulting from the liquid pressure difference between the anode and cathode can be approximated by:

$$N_{W,con} = \frac{\rho_l}{M_{H_2O}}\frac{K_{mem}}{\mu_l}\frac{(p_{l,acl/mem} - p_{l,ccl/mem})}{\delta_{mem}} \tag{21}$$

Thus, the total flux of water crossover to the cathode can be determined from:

$$N_{W,tot} = -D_{W,N}(\lambda)\nabla C_{W,N}|_{IV} + n_{d,H_2O}(\lambda)\frac{I}{F}|_{IV} + \frac{\rho_l}{M_{H_2O}}\frac{K_{mem}}{\mu_l}\frac{(p_{l,acl/mem} - p_{l,ccl/mem})}{\delta_{mem}} \tag{22}$$

2.5. Current balance and cell voltage

The protons and electrons produced by the MOR at the anode transfer to the cathode through the membrane and the external circuit, respectively. Herein, the cell current density is calculated

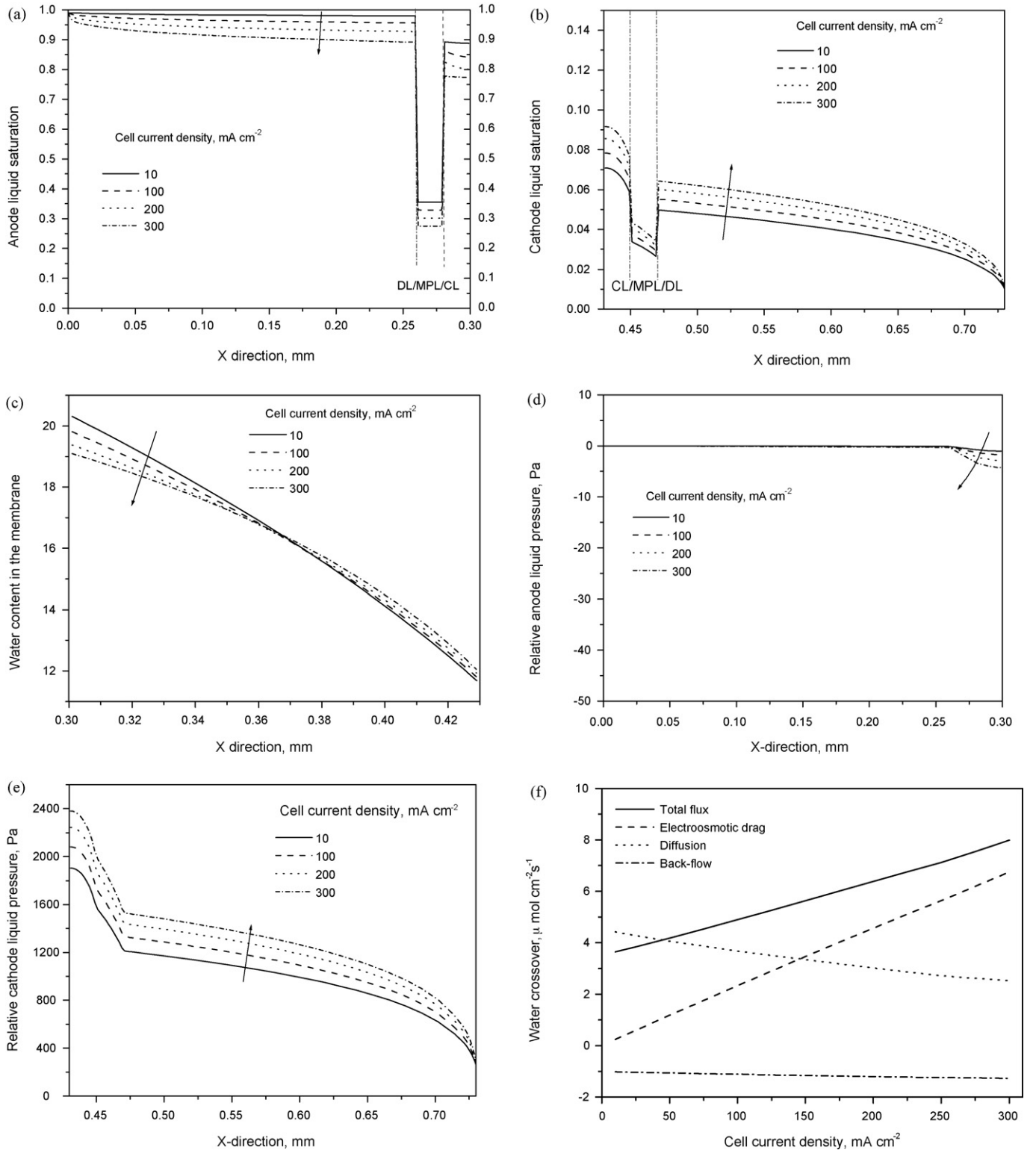

Fig. 2. Effects of current density on distributions of (a) anode liquid saturation, (b) cathode liquid saturation, (c) water content in membrane, (d) anode liquid pressure, (e) cathode liquid pressure, (f) on water crossover through membrane.

by:

$$I_{\text{cell}} = \int_{\text{acl}} j_{\text{a}} \mathrm{d}x \tag{23}$$

To account for the rate of methanol crossover, the concept of the parasitic current is used and is given by:

$$I_{\text{para}} = 6FN_{\text{M}} \tag{24}$$

where the molar flux of methanol crossover (N_M) is given by Eq. (11).

At the cathode, it is assumed both the cell current and the 'parasitic' current are completely consumed by the ORR, i.e.:

$$I_{cell} + I_{para} = \int_{ccl} j_c dx \tag{25}$$

Accordingly, for a given cell current, the anode overpotential (η_a) and the parasitic current density (I_{para}) can be calculated by Eqs. (23) and (24), respectively. Then, the cathode mixed overpotential (η_c) can be determined with the help of Eqs. (18) and (25). Finally, the cell voltage can be determined from:

$$V_{cell} = V_0 - \eta_a - \eta_c - I_{cell}\left(R_{contact} + \frac{\delta_{mem}}{\kappa}\right) \tag{26}$$

where V_0, $R_{contact}$ and κ denote the thermodynamic-equilibrium cell voltage of the DMFC, the contact resistance and the proton conductivity of the membrane, respectively.

3. Results and discussion

The above-described governing equations for the cell geometric dimensions and operating parameters listed in Table 2 subjected to the boundary conditions, along with the constitutive correlations listed in Table 1 and electrochemical properties listed in Table 3, are solved numerically using a self-written code, which was developed based on the SIMPLE algorithm with the Finite-Volume-Method [22]. Note that more details on the validation of the two-phase mass-transport model presented above can be found elsewhere [22,24].

3.1. Effect of cell current density

In this section, the distributions of several species, including liquid saturation, water content and liquid pressure, in the DMFC are presented first and then followed by the variation in the flux of water crossover with the current density.

Fig. 2a shows the distribution of the anode liquid saturation at different current densities. Interestingly, the anode liquid saturation at each interface between two adjacent layers exhibits a jump, which results from the continuity of the capillary pressure across the interface; a more detailed explanation of this phenomena has been reported me elsewhere [20]. With increase in cell current density, the anode liquid saturation level decreases as a result of increased generation of carbon dioxide (CO_2) at a higher current density. The distribution of the cathode liquid saturation at different current densities is displayed in Fig. 2b. In general, the liquid saturation level is smaller in the cathode porous region than in the anode porous region. The liquid saturation level in the cathode porous region increases with the cell current density as a result of the increased water generated in the cathode CL at a higher current density. Since the liquid saturation in the anode CL is higher than in the cathode CL at the same current density, there is a water content gradient across the membrane that can drive the water diffusion to the cathode. The distribution of the water content (equivalent to dissolved water concentration) in the membrane at different current densities is given in Fig. 2c. Apparently, there exists a large water gradient across the membrane, and this suggests that the flux of water crossover due to diffusion is substantial. For instance, at a current density of 50 mA cm^{-2}, the water content at the interface between the anode CL and the membrane is close to 20, whereas it is only about 12 at the interface between the cathode CL and the membrane. Since an increase in the current density causes the liquid saturation in the anode CL to decrease but in the cathode CL to increase (shown in Fig. 2a and b), the water gradient across the membrane becomes flatter with increasing current density, meaning that the flux of water crossover by diffusion decreases with the current density. In addition, the distribution of both the anode and cathode liquid pressure at different current densities is displayed in Fig. 2d and e, respectively. It is seen from Fig. 2d that the anode liquid pressure decreases from the anode channel to the anode CL, but the change is extremely small. On the other hand, however, Fig. 2e shows that the cathode liquid pressure decreases dramatically from the cathode CL to the cathode channel. This can be explained as follows. As indicated by Eqs. (1) and (5), the water flow through the porous medium depends on the pressure gradient, the intrinsic permeability of the porous medium, and the relative permeability. At the same current density, the relative permeability is much higher at the anode than at the cathode, as the liquid saturation at the anode is much higher than at the cathode. As a result, the pressure difference required to drive the same flux of water through the porous medium will be much higher at the cathode than at the anode. Also, it is interesting to note that the liquid pressure in the cathode CL is higher than in the anode CL, suggesting that the liquid water can flow backward from the cathode to the anode, which tends to reduce the total rate of water crossover from the anode to cathode [10–15]. In addition to the back-flow of water, however, the total rate of water crossover also depends on the electro-osmotic drag and diffusion, as follows. Fig. 2f shows the variation in the flux of water crossover due, respectively, to electro-osmotic drag, diffusion and backflow with current density. First, it is seen that the flux by electro-osmotic drag increases almost linearly with the current density, as indicated by Eq. (20). Second, it is evident that the diffusion flux is quite substantial due to the large water content gradient across the membrane, especially at low current densities. With increase in current density, the diffusion flux decreases greatly as the water content at the cathode increases with current density, whereas the water content in the anode decreases with current density. Third, the absolute value of the back-flow flux (note that a negative value means that the water flows from the cathode to anode) increases slightly with current density, as the cathode liquid pressure increases but the anode liquid pressure decreases with increasing current density. Note that the variation trends of the flux of water crossover due to each mechanism are consistent with previous experimental data [18] and numerical results [20].

In the subsequent sections, we explore how each constituent component of the MEA affects water crossover.

3.2. Effect of anode CL

In this section, we focus on investigating the effects of the contact angle and the permeability of the anode CL on water crossover. Fig. 3 shows the effect of the anode CL contact angle on the distribution of the anode liquid saturation (3a), the distribution of water content across the membrane (3b), and the rate of water crossover (3c) at a current density of 100 mA cm^{-2}. The numerical results shown in Fig. 3 were obtained by varying the contact angle from 94.5° to 99°, which indicates an increase in the anode CL hydrophobic level, while all the other parameters are kept unchanged as listed in Tables 2 and 3. As shown in Fig. 3a, an increase in the anode CL contact angle leads to a decrease in the liquid saturation level as more hydrophobic pores tend to hold more gas CO_2 in the anode CL. The decrease in liquid saturation in the anode CL directly lowers the water content in the membrane adjacent to the anode CL, as shown in Fig. 3b. It is also noticed from Fig. 3b that the water content near the cathode CL decreases slightly with increase in the anode CL contact angle. In general, Fig. 3b indicates that the water content gradient across the membrane decreases with increasing anode CL contact angle. Technically, the changes in water content and its gradient across the membrane affect water crossover through the membrane in several ways. First, a decrease in water

Table 2
Cell geometric dimensions and operating parameters.

Parameters	Symbols	Value	Unit
Anode diffusion layer thickness	δ_{adl}	2.6×10^{-4}	m
Anode microporous layer thickness	δ_{ampl}	0.2×10^{-4}	m
Anode catalyst layer thickness	δ_{acl}	0.2×10^{-4}	m
Membrane thickness	δ_{mem}	1.3×10^{-4}	m
Cathode diffusion layer thickness	δ_{cdl}	2.6×10^{-4}	m
Cathode microporous layer thickness	δ_{cmpl}	0.2×10^{-4}	m
Cathode catalyst layer thickness	δ_{ccl}	0.2×10^{-4}	m
Operation temperature	T	343.15	K
Anode inlet pressure	p_l^{in}	1.013×10^5	Pa
Cathode inlet pressure	p_g^{in}	1.013×10^5	Pa
Inlet methanol concentration at anode	C_M^{in}	1000	mol m^{-3}
Inlet methanol vapour concentration	C_{MV}^{in}	C_{MV}^{sat}	mol m^{-3}
Inlet oxygen concentration at cathode	$C_{O_2}^{in}$	7.35	mol m^{-3}
Inlet water-vapour concentration at cathode	C_{WV}^{in}	p_{WV}^{Sat}/RT	mol m^{-3}
Inlet liquid saturation at anode	s^{in}	1	–
Inlet liquid saturation at cathode	s^{in}	0	–

content decreases the diffusivity of dissolved water in the membrane, which tends to reduce the water diffusion flux through the membrane. Second, a decrease in the water-content gradient also lowers the water diffusion flux through the membrane, as indicated in Eq. (19). Third, a decrease in the water content in the membrane lowers the electro-osmotic drag coefficient of water, thus reducing the electro-osmotic drag flux, as indicated in Eq. (20). In summary, the water flux by both diffusion and electro-osmotic drag decreases with increasing anode CL contact angle. This is evident from the data in Fig. 3c. It is seen that the back-flow flux of water increases slightly with increasing the anode CL contact angle, as the liquid pressure in the cathode CL decreases slightly due to decreased liquid saturation in the cathode CL. Summarizing the water fluxes by the three mechanisms, it is found that the total rate of water crossover decreases with increasing the anode CL contact angle, as shown in Fig. 3c. That the total rate of water crossover can be reduced by almost a factor of 3 when the anode CL contact angle is changed from 94.5° to 99°. Hence, it can be concluded that increasing the hydrophobic level of the anode CL is an effective way to suppress the total rate of water crossover to the cathode.

The influence of the anode CL permeability is examined by changing its value from 0.4×10^{-14} to 3.0×10^{-14} m^2, while keeping all other parameters the same. Fig. 4a shows the distribution of anode liquid saturation with different anode CL permeabilities at a current density of 100 mA cm^{-2}. On average, the liquid saturation in the anode CL decreases from about 0.9 to 0.2 when the anode CL permeability decreases from 3.0×10^{-14} to 0.4×10^{-14} m^2. The reduction in the liquid saturation level in the anode CL from a liquid-dominant to a gas-dominant condition inevitably reduces

Table 3
Physicochemical properties.

Parameters		Symbols	Value	Unit	Ref.
	ADL	ε_{adl}, K_{adl}	0.75, 1.0×10^{-12}	–, m^2	[20]
Porosity permeability	AMPL	ε_{ampl}, K_{ampl}	0.3, 2.5×10^{-13}	–, m^2	[20]
	ACL	ε_{acl}, K_{acl}	0.3, 2.0×10^{-14}	–, m^2	
	MEM	ε_{mem}, K_{mem}	0.3, 2.0×10^{-18}	–, m^2	[20]
	CCL	ε_{ccl}, K_{ccl}	0.3, 2.0×10^{-14}	–, m^2	
	CMPL	ε_{cmpl}, K_{cmpl}	0.3, 2.5×10^{-13}	–, m^2	[20]
	CDL	ε_{cdl}, K_{cdl}	0.75, 1.0×10^{-12}	–, m^2	[20]
Nafion volume fraction in ACL		$\varepsilon_{N,acl}$	0.4	–	[33]
	MeOH in water	$D_{M,l}$	$10^{-5.4163-999.778/T}$	m^2 s^{-1}	[25]
	MeOH in Nafion	$D_{M,N}$	$4.9\times10^{-10}e^{[2436(1/333-1/T)]}$	m^2 s^{-1}	[26]
	Methanol vapour	$D_{M,g}$	$-6.954\times10^{-6}+4.5986\times10^{-8}T+9.4979\times10^{-11}T^2$	m^2 s^{-1}	[25]
Diffusivities	O_2 in gas	$D_{O_2,g}$	$1.775\times10^{-5}(T/273.15)^{1.823}$	m^2 s^{-1}	[25]
	Water-vapour	$D_{WV,g}$	$2.56\times10^{-5}(T/307.15)^{2.334}$	m^2 s^{-1}	[25]
Viscosity of gas phase		μ_g	2.03×10^{-5}	kg m^{-1} s^{-1}	[32]
Viscosity of liquid phase		μ_l	4.05×10^{-4}	kg m^{-1} s^{-1}	[32]
Electro-osmotic drag coefficients of water and methanol		n_{d,H_2O}	$2.5\lambda/22$	–	[29]
		$n_{d,M}$	$n_{d,H_2O}x_M$	–	[29]
Condensation rate constant for water		k_c	5.0×10^{-5}	mol atm^{-1} s^{-1} cm^{-3}	[27]
Evaporation rate constant for water		k_e	5.0×10^{-3}	atm^{-1} s^{-1}	[27]
Henry law constant for oxygen		k_{H,O_2}	$e^{(-666/T+14.1)}/R/T$	–	[30]
Henry law constant for methanol		$k_{H,M}$	$0.096e^{0.04511(T-273)}$	atm	[25]
Interfacial transfer rate constant for methanol		h_{lg}	0.001	m^2 s^{-1}	[28]
Specific interfacial area between liquid and gas		A_{lg}	10^5	m^{-1}	[28]
Proton conductivity in membrane		κ	$7.3e^{[1268(1/298-1/T)]}$	Ω^{-1} m^{-1}	[26]
The saturation pressure of water vapour		$\log_{10}p_{WV}^{sat}$	$-2.1794+0.02953(T-273)-9.1837\times10^{-5}(T-273)^2+1.4454\times10^{-7}(T-273)^3$	atm	[31]
The saturation pressure of methanol vapour		p_{MV}^{sat}	$k_{H,M}x_{M,l}$	atm	[25]
Thermodynamic voltage		V_0	1.21	V	[25]
Transfer coefficient of anode		α_a	0.5	–	[22]
Transfer coefficient of cathode		α_c	1.0	–	[22]
Athode exchange current density		$A_{v,a}j_{0,M}^{ref}$	1.0×10^5	A m^{-3}	[22]
Cathode exchange current density		$A_{v,c}j_{0,O_2}^{ref}$	1.14×10^3	A m^{-3}	[22]
Anode reference concentration		C_M^{ref}	100	mol m^{-3}	[22]
Cathode reference concentration		$C_{O_2}^{ref}$	0.52	mol m^{-3}	[22]
Surface tension		σ	0.0644	N m^{-1}	[32]
Equivalent weight of ionomer		EW	1.1	kg mol^{-1}	[34]
Dry membrane density		ρ_{dry}	1980	kg m^3	[34]

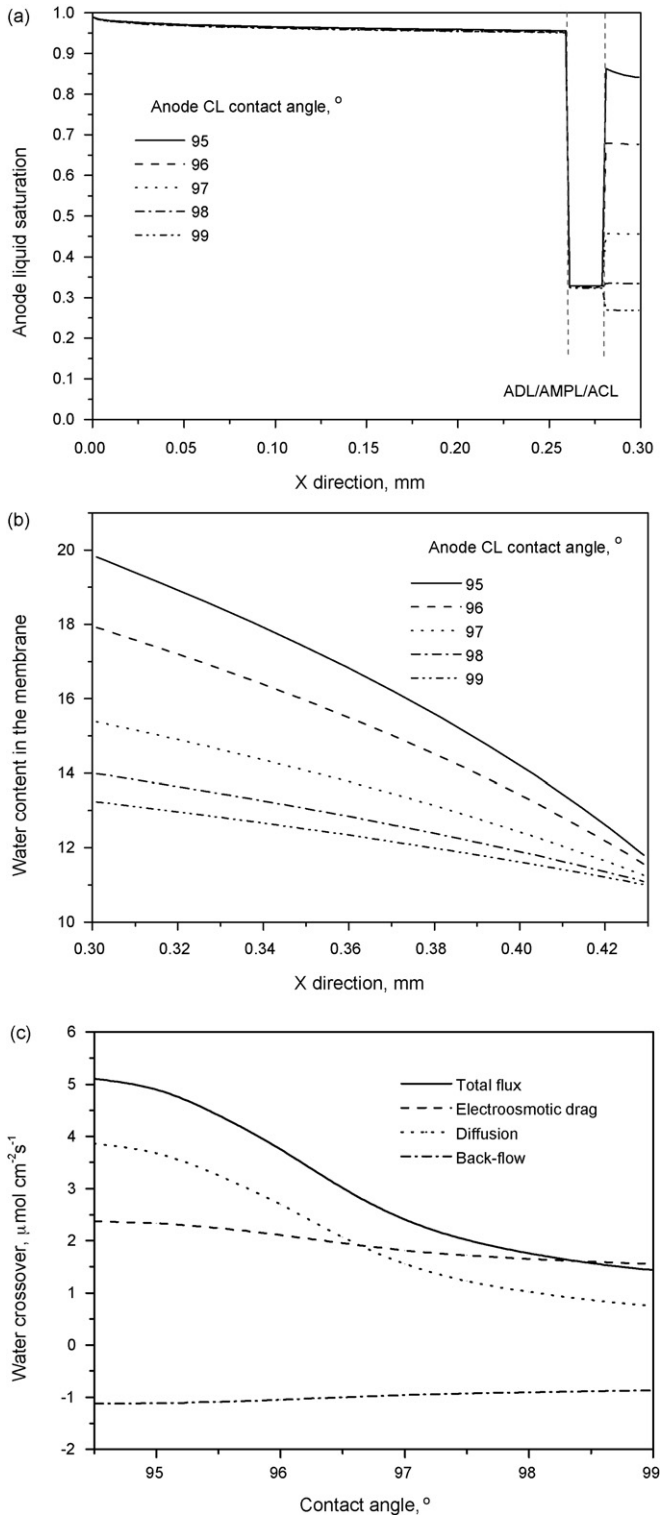

Fig. 3. Effect of anode CL contact angle on (a) distribution of anode liquid saturation, (b) distribution of water content in membrane, (c) water crossover through membrane.

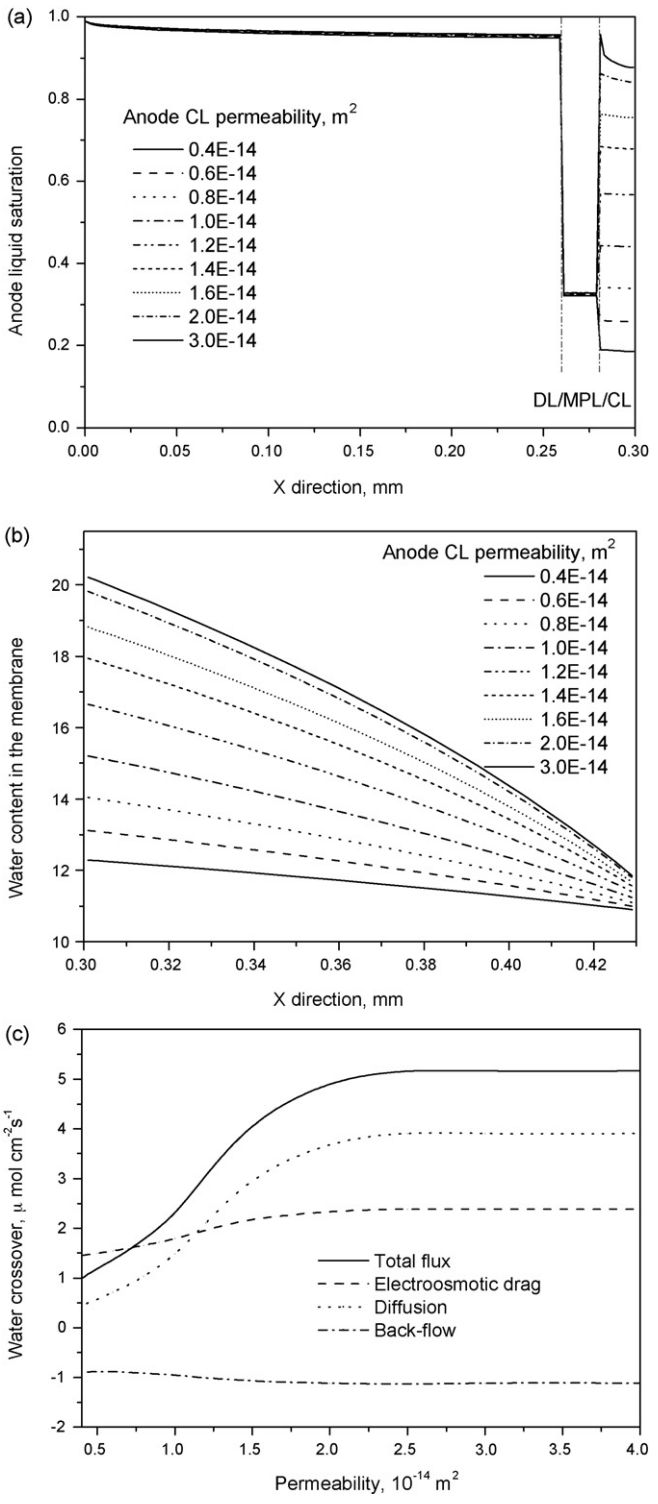

Fig. 4. Effect of anode CL permeability on (a) distribution of anode liquid saturation, (b) distribution of water content in membrane, (c) water crossover through the membrane.

the water content level in the membrane and its gradient across the membrane. As indicated in Fig. 4b, the water content in the membrane near the anode CL decreases from about 20 to about 12 when the anode CL permeability decreases from 3.0×10^{-14} to 0.4×10^{-14} m^2. Fig. 4b also shows that the water-content gradient across the membrane decreases with decreasing anode CL permeability. As discussed earlier, the decrease in the water content and its gradient across the membrane reduces both the diffusion and the electro-osmotic drag flux of water through the membrane. As shown in Fig. 4c, the diffusion flux decreases by a factor of almost 7 when decreasing the anode CL permeability from 3.0×10^{-14} to 0.4×10^{-14} m^2. In the meantime, the electro-osmotic drag flux decreases with decreasing anode CL permeability. As for the absolute value of the back-flow flux, it slightly decreases with decreasing anode CL permeability due to the lowered cathode liq-

uid pressure. Overall, the total rate of water crossover decreases by a factor of about 5 when decreasing the anode CL permeability from3.0×10^{-14} to 0.4×10^{-14} m^2. Hence it can be concluded that water crossover can be effectively suppressed by lowering the anode CL permeability, which can be achieved by reducing the pore size of the anode CL.

3.3. Effect of anode MPL

First, we investigate how the anode MPL contact angle affects water transport through the MEA. Fig. 5a shows the distribution of anode liquid saturation with different anode MPL contact angles at a current density of 100 mA cm^{-2}. As can be seen, an increase in anode MPL contact angle leads to a significant reduction in liquid saturation in the anode MPL, but liquid saturation in the anode CL remains almost the same value. As a result, a change in anode MPL contact angle does not alter the water content gradient across the membrane, as shown in Fig. 5b. Accordingly, as shown in Fig. 5c, the water fluxes by all the three mechanisms do not change with a change in anode MPL contact angle. Hence, it can be concluded that the anode MPL contact angle has little effect on water crossover. Nevertheless, it should be mentioned that increasing the anode MPL contact angle will lead to an increase in the mass-transport resistance of liquid methanol in the anode MPL, as a result of the decreased liquid saturation there, and this would be a benefit to the use of more concentrated methanol solutions in DMFCs.

The influence of anode MPL permeability is examined by increasing its value from 0.25×10^{-14} to 4.0×10^{-14} m^2. Fig. 6a presents the distribution of anode liquid saturation with different permeabilities at a current density of 100 mA cm^{-2}. It is seen that liquid saturation in the anode MPL decreases greatly with decreasing anode MPL permeability, but the change in the liquid saturation in the anode CL is much smaller. The corresponding distribution of water content across the membrane is displayed in Fig. 6b. The water content in the membrane near the anode CL decreases slightly as a result of the decreased liquid saturation in the anode CL, which, in turn, results in a slight decrease in the water content gradient across the membrane. As a result, as shown in Fig. 6c, the diffusion flux of water decreases slightly when the anode MPL permeability is decreased from 1.0×10^{-14} to 0.25×10^{-14} m^2. In summary, the anode MPL permeability has little effect on water crossover. It is worth mentioning that decreasing the anode MPL permeability will also cause an increase in the mass-transport resistance of liquid methanol, which results from the decreased liquid saturation in the anode MPL.

3.4. Effect of cathode CL

In this section, the effects of two cathode CL parameters, namely the contact angle and the permeability, on water transport through the MEA are examined. The cathode CL contact angle was varied from 94° to 99°. Fig. 7a shows the distribution of the cathode liquid pressure with different contact angles at a current density of 100 mA cm^{-2}. As can be seen, an increase in cathode CL contact angle leads to a sharper increase in liquid pressure across the cathode CL. This implies that the liquid pressure in the cathode CL can be enhanced by increasing the cathode CL hydrophobic level. The corresponding distribution of the cathode liquid saturation is given in Fig. 7b, which indicates that the liquid saturation in the cathode CL decreases with increasing cathode CL contact angle. Hence, increasing the cathode CL hydrophobic level can not only build up a higher liquid pressure but can also help to reduce the liquid saturation in the cathode CL. The effect of the cathode CL contact angle on water crossover through the membrane is presented in Fig. 7c. It is seen that increasing the cathode CL contact angle enhances the back-flow of water, thus suppressing water crossover. Overall,

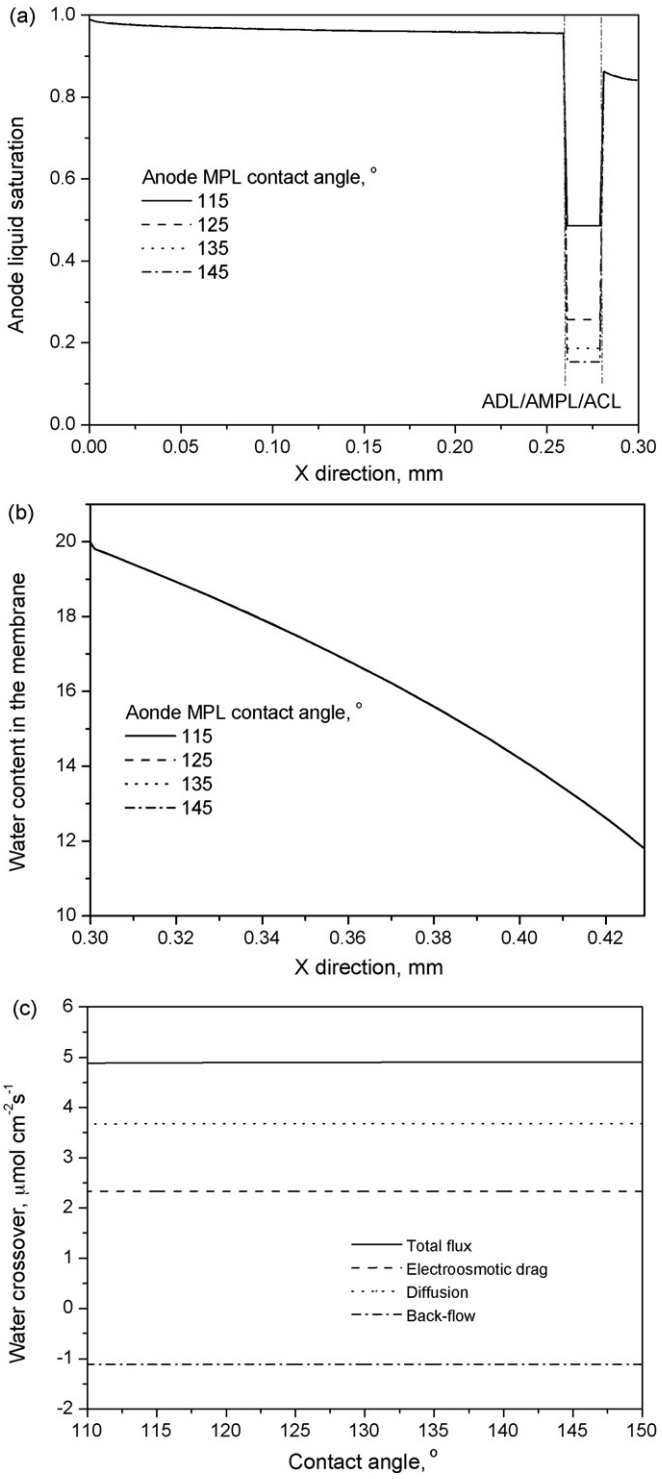

Fig. 5. Effect of anode MPL contact angle on (a) distribution of anode liquid saturation, (b) distribution of water content in membrane, and (c) water crossover through membrane.

the total rate of water crossover decreases with increasing cathode CL contact angle. Hence, it can be concluded that increasing the cathode CL contact angle is a benefit not only to lowering water crossover, but also to water flooding avoidance in the cathode CL.

The influence of cathode CL permeability is examined by varying its value from 0.3×10^{-14} to 5.0×10^{-14} m^2. Fig. 8a shows the distributions of the cathode liquid pressure with different cathode CL permeabilities at a current density of 100 mA cm^{-2}. Clearly, the

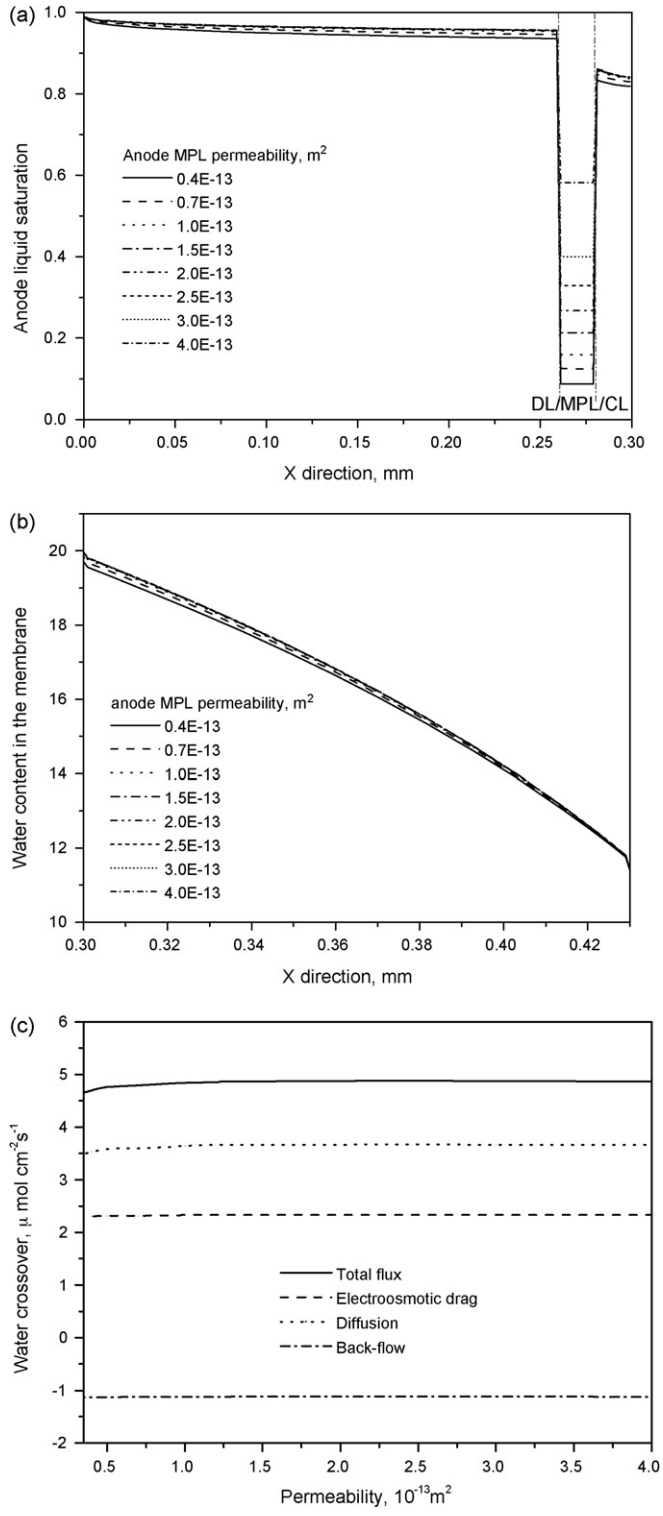

Fig. 6. Effect of anode MPL permeability on (a) distribution of anode liquid saturation, (b) distribution of water content in membrane, (c) water crossover through membrane.

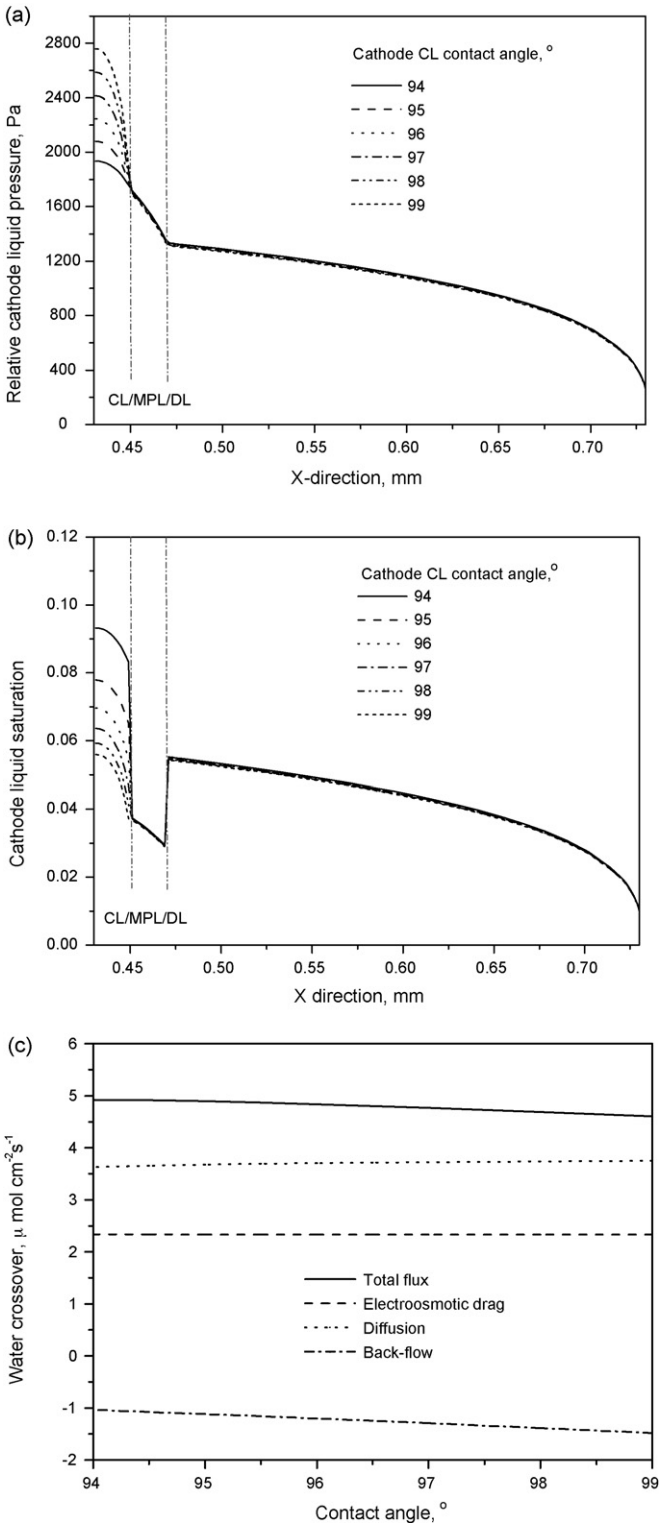

Fig. 7. Effect of cathode CL contact angle on (a) distribution of cathode liquid pressure, (b) distribution of cathode liquid saturation, (c) water crossover through membrane.

liquid pressure across the cathode CL increases more rapidly with decreasing cathode CL permeability. For increase, the liquid pressure increases from about 1.6 to 4.5 kPa across the cathode CL for a permeability of 0.4×10^{-14} m^2. This result indicates that decreasing the cathode CL permeability helps build up a high liquid pressure in the cathode CL. The corresponding distributions of the liquid saturation in the cathode are shown in Fig. 8b. In general, the change in the liquid saturation in the cathode CL is small with decreasing cathode CL permeability, thus causing little effect on the distribution of the water content in the membrane. The dependence of water crossover on cathode CL permeability is shown in Fig. 8c. Clearly, both the water fluxes by diffusion and electro-osmotic drag remain almost unchanged with permeability. On the other hand, the back-flow of water is greatly enhanced with reduction in cathode

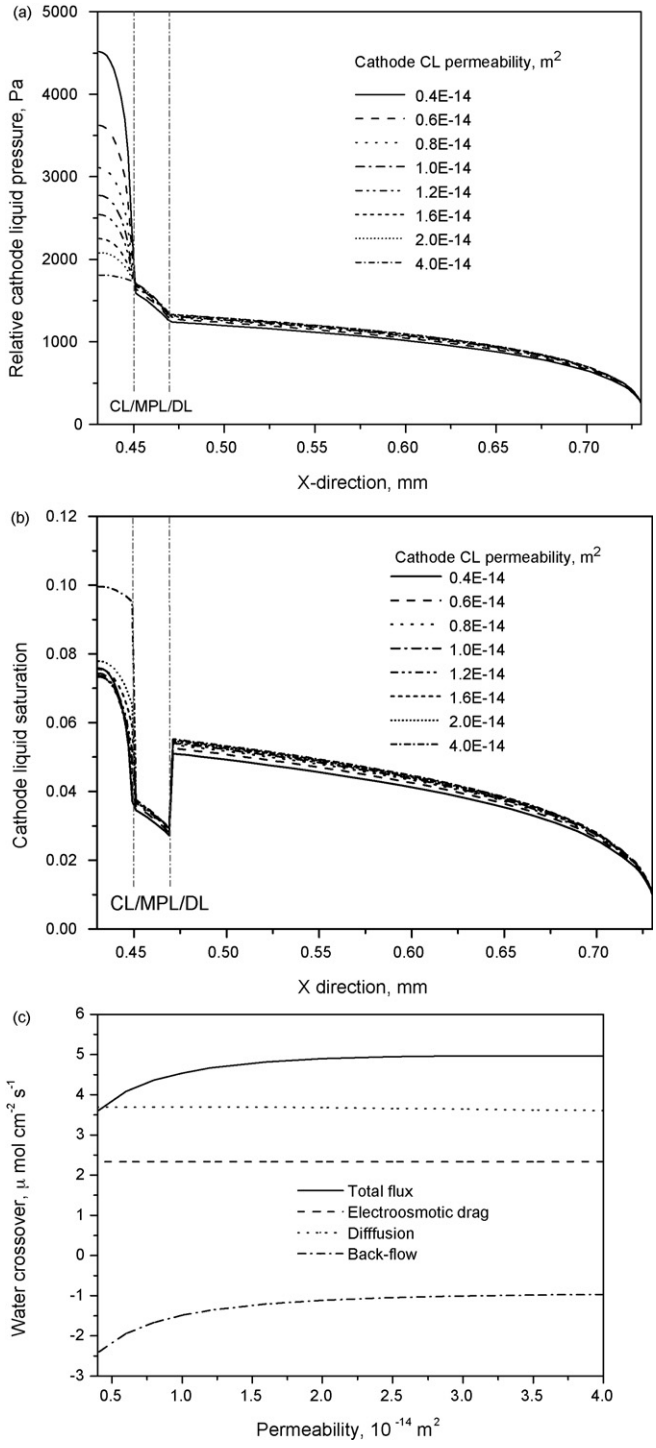

Fig. 8. Effect of cathode CL permeability on (a) distribution of cathode liquid pressure, (b) distribution of cathode liquid saturation, (c) water crossover through membrane.

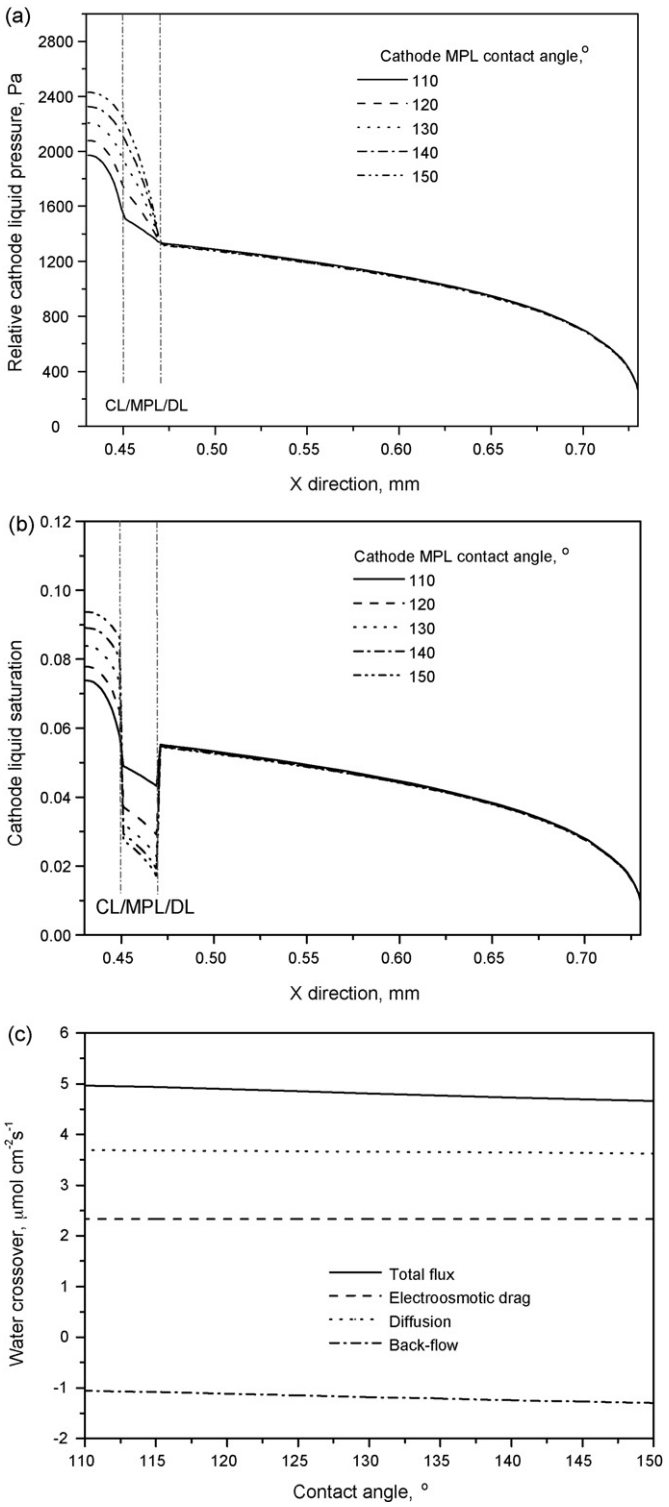

Fig. 9. Effect of the cathode MPL contact angle on (a) the distribution of cathode liquid pressure, (b) the distribution of cathode liquid saturation, and (c) water crossover through the membrane.

CL permeability. As a result, the total rate of water crossover to the cathode is reduced from 5.0 to 3.5 $\mu mol\,cm^{-2}\,s^{-1}$ when decreasing the cathode CL permeability from 2.0×10^{-14} to $0.4 \times 10^{-14}\,m^2$. Hence, decreasing the cathode CL permeability is also effective in suppressing water crossover in DMFCs.

3.5. Effect of cathode MPL

In this section, first we investigate the effect of the cathode MPL contact angle on water transport through the MEA, followed by examining the effect of cathode MPL permeability. The cathode MPL contact angle is varied from 110° to 150°. Fig. 9a shows the distribution of cathode liquid pressure with different cathode

MPL contact angles at a current density of 100 mA cm^{-2}. Clearly, the gradient of liquid pressure across the cathode MPL becomes relatively larger with increasing cathode MPL hydrophobic level, which, in turn, results in a slight increase in the liquid pressure in the cathode CL. The corresponding distribution of cathode liquid saturation with different cathode MPL contact angles is shown in Fig. 9b. As can be seen, the mean liquid saturation in the cathode MPL decreases from about 0.045 to about 0.025 when increasing the cathode MPL contact angle from 110° to 150°, but the mean liquid saturation in the cathode CL increases slightly from about 0.07 to about 0.09 as a result of increased liquid pressure in the cathode CL. Fig. 9c displays the effect of the cathode MPL contact angle on water crossover. The absolute value of the back-flow flux of water slightly increases with increasing cathode MPL contact angle as a result of the slightly enhanced liquid pressure in the cathode CL. Overall, the total rate of water crossover decreases with increasing contact angle, but the change is relatively small. This is probably due to the two reasons. First, the built up of liquid pressure in the cathode MPL is relatively insensitive to the contact angle of the cathode MPL once the hydrophobic level is high enough in the cathode MPL, as indicated in Eq. (9), such that the back-flow flux is not sensitive to the increase in the contact angle of the hydrophobic cathode MPL. Second, the flux of water crossover to the cathode due to diffusion and electro-osmotic drag is so strong that the enhancement in the back-flow flux can only offset a small portion of the water crossover by diffusion and electro-osmotic drag [19–20].

The influence of the cathode MPL permeability is examined by varying its value from 4.0×10^{-13} to 0.4×10^{-13} m^2. Fig. 10a shows the distribution of cathode liquid pressure with different cathode MPL permeabilities at a current density of 100 mA cm^{-2}. Clearly, the liquid pressure across the cathode MPL increases sharply with decreasing the cathode MPL permeability. For instance, the liquid pressure increases from about 1.0 to 3.9 kPa across the cathode MPL for a permeability of 0.4×10^{-13} m^2. As a result, the liquid pressure in the cathode CL is significantly enhanced on decreasing the cathode MPL permeability. The corresponding distribution of liquid saturation in the cathode is presented in Fig. 10b. On decreasing the cathode MPL permeability from 4.0×10^{-13} to 0.4×10^{-13} m^2, the liquid saturation in the cathode MPL and the cathode DL decreases slightly, but the liquid saturation in the cathode CL increases greatly from about 0.07 to about 0.17 as a result of the significantly increased liquid pressure in the cathode CL as shown in Fig. 10a. Due to the changes in liquid pressure and liquid saturation in the cathode CL that result from the change in the cathode MPL permeability, the water crossover through the membrane will be affected. The dependence of water crossover on cathode MPL permeability is presented in Fig. 10c. As shown, the total rate of water crossover decreases slightly when the cathode MPL permeability decreases from 4.0×10^{-13} to 1.0×10^{-13} m^2, but it decreases sharply when the permeability falls below 1.0×10^{-13} m^2. Obviously, the rapid decrease in the total rate of water crossover is mainly caused by the enhanced back-flow of water. In addition, the diffusion flux of water decreases slightly as a result of increased liquid saturation in the cathode CL. Although decreasing the cathode MPL permeability tends to reduce water crossover, the induced relatively high liquid saturation in the cathode CL might cause an adverse impact on oxygen transport in the cathode CL, which may lower the cathode potential. Therefore, a careful optimization of the cathode MPL is necessary to balance the two opposite effects in real applications.

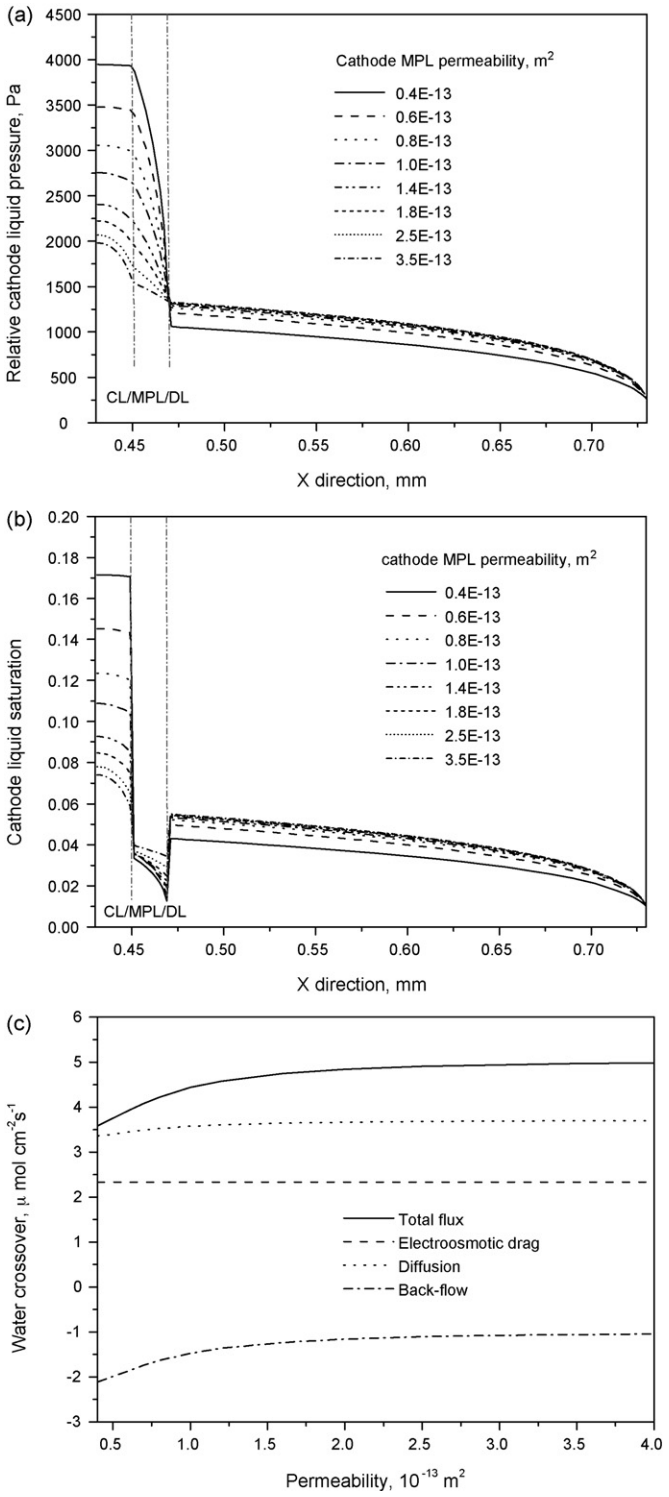

Fig. 10. Effect of the cathode MPL permeability on (a) the distribution of cathode liquid pressure, (b) the distribution of cathode liquid saturation, and (c) water crossover through the membrane.

3.6. Effect of membrane

In this section, the influence of two membrane parameters, namely thickness and permeability, on water crossover is examined. The fluxes of water crossover through different membranes (including Nafion 112, Nafion 115 and Nafion 117) at a current density of 100 mA cm^{-2} are presented in Fig. 11. It is seen that the total rate of water crossover through a thicker membrane is much lower than that through a thinner one. For instance, the flux of water crossover decreases from about 10 to 5 μmol cm^{-2} s^{-1} when the Nafion 112 membrane is replaced by Nafion 115 membrane. As indicated in Eqs. (19) and (21), an increase in membrane thickness will result in a decrease in both the diffusion flux and back-flow flux of

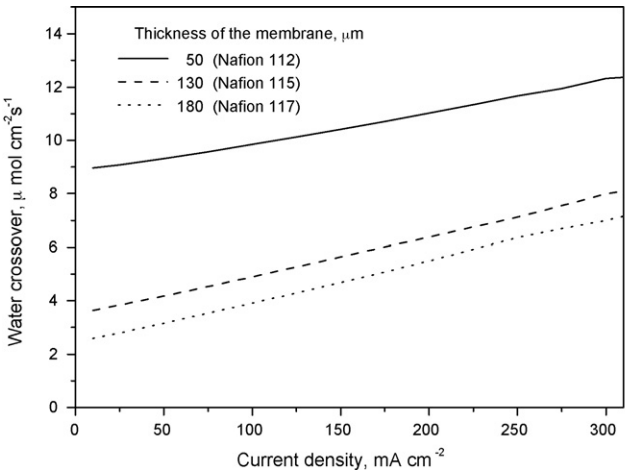

Fig. 11. Effect of the membrane thickness on water crossover through the membrane.

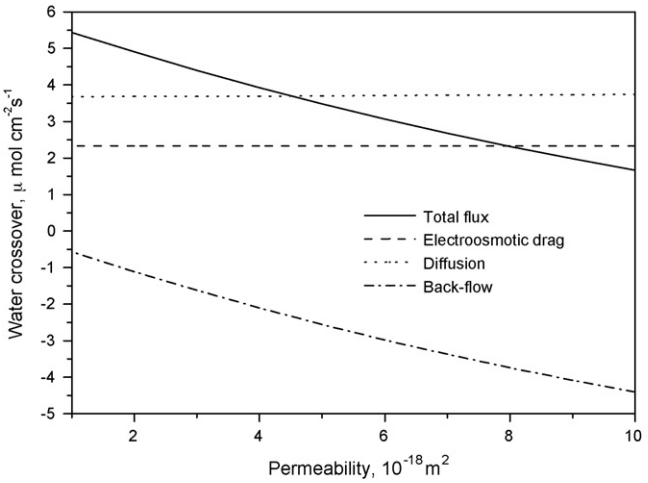

Fig. 12. Effect of the membrane permeability on water crossover through the membrane.

water crossover through the membrane. Since the diffusion flux is much higher than the back-flow flux of water in this study, employing a thick membrane can effectively reduce the total rate of water crossover as well as the rate of methanol crossover, which tends to reduce the anode water loss, mitigate the cathode water flooding, and simultaneously lower the cathode mixed over potential. On the other hand, a penalty associated with the thick membrane is the high ohmic loss of the cell. Thus there is a tradeoff of benefits and disadvantages in real applications. Also, it is worth mentioning that, in some special cases where the water diffusion is much weaker than the water back-flow through the membrane or both are in the same direction from the cathode to the anode, the use of thinner membrane is preferred [14–15,18].

The influence of membrane permeability on water crossover is examined by varying its value from 1×10^{-18} to 1×10^{-17} m^2. Fig. 12 presents the effect of the membrane permeability on water crossover at a current density of 100 mA cm^{-2}. It is seen that the back-flow flux of water increases from 0.5 to 4.0 μmol cm^{-2} s^{-1} when the membrane permeability is increased from 1×10^{-18} to 1×10^{-17} m^2. As a result, the total rate of water crossover decreases greatly as a result of the enhanced back-flow flux of water. This result suggests that the membrane permeability should be as high as possible for enhancing the back-flow of water to the DMFC anode.

4. Conclusions

In this work, a two-phase mass-transport model is used to investigate the water transport through the MEA of a DMFC. The effects of the design variables of each constituent component of the MEA on each of the three water crossover mechanisms, namely electro-osmotic drag, diffusion and back-flow, have been examined. Key parameters that influence water crossover have been identified. The salient findings are summarized as follows.

(1) Liquid saturation in the anode CL is usually larger than that in the cathode CL, especially at low current densities, and results in a water content gradient across the membrane to drive the water diffusion to the cathode. On the other hand, the liquid pressure in the cathode is larger in the anode, leading to a back-flow of water from the cathode to the anode. Increasing the cell current density leads to a decrease in the liquid saturation in the anode CL as a result of the increased generation rate of CO_2, which decreases the water diffusion through the membrane. On the other hand, the liquid pressure in the cathode CL increases with current density, resulting in an increase in the back-flow of water through the membrane. Technically, lowering the diffusion flux of water to the cathode or enhancing the back-flow of water to the anode can reduce the total rate of water crossover in the DMFC.
(2) Lowering the liquid saturation in the anode CL by decreasing the anode CL permeability or increasing the anode CL hydrophobic level can greatly reduce the water content and its gradient across the membrane, thereby reducing the diffusion flux and electro-osmotic drag flux of water across the membrane. As a result, the total rate of water crossover can be significantly suppressed. By contrast, anode MPL permeability and contact angle have little effect on water crossover through the membrane.
(3) The permeability and contact angle of both the cathode CL and cathode MPL are found to have strong impacts on water crossover in the DMFC. Lowering the permeability or increasing the contact angle can help the build up of a high liquid pressure in the cathode CL, thus enhancing the back-flow of water to the anode and reducing the total rate of water crossover.
(4) Increasing the thickness and permeability of the membrane can greatly lower the total rate of water crossover to the cathode. Although employing a thicker membrane helps reduce water crossover and methanol crossover, a penalty associated with the use of thicker membranes is the higher cell resistance, which lowers cell performance. Attention needs to be paid to a tradeoff between the benefits and disadvantages in real applications. It should be noted that in some special cases where the water diffusion is much weaker than the water back-flow through the membrane or both are in the same direction from the cathode to the anode, the use of a thinner membrane is preferred.

Acknowledgements

The work described in this paper was fully supported by a grant from the Research Grants Council of the Hong Kong Special Administrative Region, China (project no. 622807) and by the Joint Research Fund for Hong Kong and Macao Young Scholars (project no. 50629601).

References

[1] H. Yang, T.S. Zhao, Q. Ye, J. Power Sources 139 (2005) 79.
[2] C. Xu, T.S. Zhao, Q. Ye, Electrochim. Acta 51 (2006) 5524.
[3] C. Xu, T.S. Zhao, Electrochem. Commun. 9 (2007) 493.
[4] X. Ren, W. Henderson, S. Gottesfeld, J. Electrochem. Soc. 144 (1997) L267.
[5] X. Ren, S. Gottesfeld, J. Electrochem. Soc. 148 (2001) A87.
[6] S. Ge, B. Yi, P. Ming, J. Electrochem. Soc. 153 (2006) A1443.

[7] J. St-Pierre, J. Electrochem. Soc. 154 (2007) B88.
[8] T. Schultz, K. Sundmacher, J. Membr. Sci. 276 (2006) 272.
[9] W.P. Lu, C.Y. Wang, J. Power Sources 164 (2004) 189.
[10] E. Peled, A. Blum, A. Aharon, M. Philosoph, Y. Lavi, Electrochem. Solid State Lett. 6 (2003) A268.
[11] A. Blum, T. Duvdevani, M. Philosoph, N. Rudoy, E. Peled, J. Power Sources 117 (2003) 22.
[12] H. Kim, J. Oh, J. Kim, H. Chang, J. Power Sources 162 (2006) 497.
[13] G. Jewett, Z. Guo, A. Faghri, J. Power Sources 168 (2007) 434.
[14] G.Q. Lu, F.Q. Liu, C.Y. Wang, Electrochem. Solid State Lett. 8 (2005) A1.
[15] F.Q. Liu, G.Q. Lu, C.Y. Wang, J. Electrochem. Soc. 153 (2006) A543.
[16] R. Jiang, D. Chu, J. Electrochem. Soc. 155 (2008) B798.
[17] R. Jiang, D. Chu, J. Electrochem. Soc. 155 (2008) B804.
[18] C. Xu, T.S. Zhao, J. Power Sources 168 (2007) 143.
[19] C. Xu, T.S. Zhao, J. Power Sources 171 (2007) 268.
[20] C. Xu, T.S. Zhao, W.W. Yang, J. Power Sources 178 (2008) 291.
[21] F.Q. Liu, C.Y. Wang, Electrochim. Acta 53 (2008) 5517.
[22] W.W. Yang, T.S. Zhao, Electrochim. Acta 52 (2007) 6125.
[23] W.W. Yang, T.S. Zhao, J. Power Sources 174 (2007) 136.
[24] W.W. Yang, T.S. Zhao, Electrochim. Acta 53 (2007) 853.
[25] Z.H. Zhang, C.Y. Wang, J. Electrochem. Soc. 150 (2003) A508.
[26] K. Scott, W.M. Taama, J. Cruichshank, J. Power sources 65 (1997) 159.
[27] G. Murgia, L. Pisani, A.K. Shula, K. Scott, J. Electrochem. Soc. 150 (2003) A1231.
[28] J. Divisek, J. Fuhrmann, K. Gartner, R. Jung, J. Electrochem. Soc. 150 (2003) A811.
[29] X. Ren, T.E. Springer, T.A. Zawodzinski, S. Gottesfeld, J. Electrochem. Soc. 147 (2000) 466.
[30] D. Song, Q. Wang, Z. Liu, T. Navessin, M. Eikerling, S. Holdcroft, J. Power Sources 126 (2004) 104.
[31] A. Kazim, H.T. Liu, P. Forges, J. Appl. Electrochem. 29 (1999) 1409.
[32] W.W. Yang, T.S. Zhao, Y.L. He, J. Power Sources 185 (2008) 765.
[33] W.W. Yang, T.S. Zhao, J. Power Sources 185 (2008) 1131.
[34] H. Meng, C.Y. Wang, J. Electrochem. Soc. 151 (2004) A358.